



**HAL**  
open science

## Dynamics of the localization of the plastid terminal oxidase PTOX inside the chloroplast

Susanne Bolte, Elodie Marcon, Mélanie Jaunario, Lucas Moyet, Marie-Thérèse Paternostre, Marcel Kuntz, Anja Krieger-Liszkay

### ► To cite this version:

Susanne Bolte, Elodie Marcon, Mélanie Jaunario, Lucas Moyet, Marie-Thérèse Paternostre, et al.. Dynamics of the localization of the plastid terminal oxidase PTOX inside the chloroplast. *Journal of Experimental Botany*, 2020, 71 (9), pp.2661-2669. 10.1093/jxb/eraa074 . hal-02495692

**HAL Id: hal-02495692**

**<https://hal.science/hal-02495692v1>**

Submitted on 20 Oct 2020

**HAL** is a multi-disciplinary open access archive for the deposit and dissemination of scientific research documents, whether they are published or not. The documents may come from teaching and research institutions in France or abroad, or from public or private research centers.

L'archive ouverte pluridisciplinaire **HAL**, est destinée au dépôt et à la diffusion de documents scientifiques de niveau recherche, publiés ou non, émanant des établissements d'enseignement et de recherche français ou étrangers, des laboratoires publics ou privés.

1 **Dynamics of the localization of the plastid terminal oxidase PTOX inside the chloroplast**

2

3 Susanne Bolte<sup>1</sup>, Elodie Marcon<sup>2</sup>, Mélanie Jaunario<sup>2</sup>, Lucas Moyet<sup>3</sup>, Marie-Thérèse  
4 Paternostre<sup>2</sup>, Marcel Kuntz<sup>3</sup>, Anja Krieger-Liszkay<sup>2,\*</sup>

5

6 <sup>1</sup>Sorbonne Université, CNRS-FRE 3631 - Institut de Biologie Paris Seine, Imaging Core  
7 Facility, Paris, France

8 <sup>2</sup>Université Paris-Saclay, CEA, CNRS, Institute for Integrative Biology of the Cell (I2BC),  
9 91198, Gif-sur-Yvette cedex, France

10 <sup>3</sup> Cell & Plant Physiology Laboratory, Université Grenoble Alpes, CNRS, INRA, CEA, 17-  
11 Rue des Martyrs, 38054 Grenoble cedex 9, France

12

13

14 \*Author for correspondence: Anja Krieger-Liszkay; e-mail [anja.krieger-liszkay@cea.fr](mailto:anja.krieger-liszkay@cea.fr)

15

16

17 **Running title:** Localization of the plastid terminal oxidase

18

19

20 **High light**

21 We demonstrate that plastid terminal oxidase (PTOX) localization to the thylakoid membrane  
22 depends on pH and ionic strength using in vitro reconstitution assays and GFP-labelled PTOX  
23 in confocal microscopy.

24

25

26 Word count: 4433

27

28

29 **Abstract**

30 The plastid terminal oxidase (PTOX) is a plastoquinone:plastoquinone oxidoreductase that  
31 shares structural similarities with alternative oxidases (AOX). Multiple roles have been  
32 attributed to PTOX, such as involvement in carotene desaturation, a safety valve function,  
33 participation in the processes of chlororespiration and setting the redox poise for cyclic electron  
34 transport. PTOX activity has been previously shown to depend on its localization at the  
35 thylakoid membrane. Here we investigated the dynamics of PTOX localization in dependence  
36 on the proton motive force. Infiltrating illuminated leaves with uncouplers led to a partial  
37 dissociation of PTOX from the thylakoid membrane. In vitro reconstitution experiments  
38 showed that the attachment of purified recombinant MBP-OsPTOX to liposomes and isolated  
39 thylakoid membranes was strongest at slightly alkaline pH values in the presence of lower  
40 millimolar concentrations of KCl or MgCl<sub>2</sub>. In *A. thaliana* overexpressing GFP-PTOX,  
41 confocal microscopy images showed that PTOX formed distinct spots in chloroplasts of dark-  
42 adapted or uncoupler-treated leaves while the protein was more equally distributed in a  
43 network-like structure in the light. We propose a dynamic PTOX association with the thylakoid  
44 membrane depending on the presence of a proton motive force.

45

46 **Keywords:** alternative electron transport; chloroplast; confocal microscopy; liposomes;  
47 membrane association; plastid terminal oxidase

48

49

50

51

## 52 **Introduction**

53 The plastid terminal oxidase (PTOX) is a non-heme diiron quinol oxidase that oxidizes  
54 plastoquinol and reduces O<sub>2</sub> to H<sub>2</sub>O. PTOX was discovered in the so-called *immutans* mutant  
55 of *A. thaliana* showing a variegated phenotype (Wetzel et al., 1994; Carol et al., 1999). This  
56 enzyme is involved in carotenoid biosynthesis, plastid development, chlororespiration, and it  
57 has been proposed to act as a safety valve by protecting the plastoquinone pool from  
58 overreduction under abiotic stress. *A. thaliana* grown in moderate light under non-stress  
59 conditions have low PTOX concentrations (about 1 PTOX protein per 100 PSII; Lennon et al.,  
60 2003). By contrast, elevated PTOX levels have been found in certain species exposed to abiotic  
61 stresses such as high temperatures, high light and drought (Quiles, 2006), salinity (Stepien and  
62 Johnson, 2009; 2018), low temperatures, and high intensities of visible (Ivanov et al., 2012)  
63 and UV light (Laureau et al., 2013).

64 It is generally accepted that in most plant species PTOX has low activity compared to  
65 photosynthetic electron flow. The maximum rate of PTOX was reported to be 5 e<sup>-</sup> s<sup>-1</sup> per PSII  
66 for PTOX2 in *C. reinhardtii* and 0.3 e<sup>-</sup> s<sup>-1</sup> PSII<sup>-1</sup> in tomato (Trouillard et al., 2012), while the  
67 maximal rate of photosynthesis is approximately 150 e<sup>-</sup> s<sup>-1</sup> per PSII (Nawrocki et al., 2015).  
68 However, in *Eutrema salsugineum* exposed to stress, PTOX activity can account for 30% of  
69 the PSII activity (Stepien and Johnson, 2009). The *in vitro* enzyme activity of recombinant  
70 PTOX (MBP-OsPTOX) from rice is high (up to 19.01 ± 1.1 μmol O<sub>2</sub> mg protein<sup>-1</sup> min<sup>-1</sup>; Yu  
71 et al., 2014). The discrepancy between the reported PTOX activities *in planta* and the V<sub>max</sub>  
72 measured with the purified protein points to a mechanism that allows the regulation of PTOX  
73 activity depending on the reduction state of the electron transport chain.

74 Since PTOX may compete with linear and cyclic electron flow (Feilke et al., 2016;  
75 Krieger-Liszky and Feilke, 2016), a highly active or highly abundant PTOX may negatively  
76 impact ATP and NADPH production. To avoid interference of PTOX activity with  
77 photosynthetic electron transport under conditions favorable for CO<sub>2</sub> assimilation, its activity  
78 must be tightly controlled. High PTOX activity seems to be beneficial for the plant to protect  
79 the photosynthetic apparatus against photoinhibition when the electron transport chain is in a  
80 highly reduced state, as it is the case under abiotic stress like high salinity, drought, or when  
81 CO<sub>2</sub> fixation is limited by unfavorable temperatures. However, high PTOX activity is  
82 detrimental to high photosynthetic activity when light and CO<sub>2</sub> are not limiting.

83 PTOX has been localized in spinach chloroplasts of non-stressed leaves in the non-  
84 appressed regions of the thylakoid membrane (Lennon et al., 2003). We have proposed  
85 previously a model suggesting that PTOX attachment to the thylakoid membrane depends on

86 the proton motive force (Krieger-Liszkay and Feilke, 2016). According to this model, PTOX is  
87 attached to the membrane in high light when both  $\Delta\text{pH}$  (the proton gradient) and  $\Delta\psi$  (the  
88 membrane potential) across the thylakoid membrane are high. Changes of the localization of  
89 PTOX would regulate PTOX activity by either allowing or by restricting its access to its  
90 substrate. We have shown previously that PTOX was associated to thylakoid membrane  
91 isolated from leaves exposed to high light, but not in those isolated from dark-adapted leaves.  
92 In dark-adapted leaves PTOX was mostly found in the fraction of soluble proteins (Feilke et  
93 al., 2016). Recently another type of regulation also based on changes in PTOX localization has  
94 been described in *Eutrema salsugineum* exposed to salt stress. In control conditions, PTOX was  
95 localized at the unstacked stroma lamellae where it has no access to its substrate plastoquinol  
96 while in plants exposed to salt stress it was translocated to the grana stacks (Stepien and  
97 Johnson, 2018). Stepien and Johnson (2018) proposed that PTOX not only translocates from  
98 the stroma lamellae to the grana stacks but may also moves across the thylakoid membrane to  
99 the lumen side and is active in the lumen.

100 Here we studied the effect of the proton motive force on PTOX attachment to the  
101 membrane by different approaches. We infiltrated leaves with uncouplers and determined the  
102 PTOX localization by immunoblots. In addition, we adsorbed recombinant MBP-OsPTOX to  
103 liposomes or thylakoid membranes at different pH values and different ion concentrations.  
104 Confocal microscopy images revealed differences in the localization of GFP-PTOX between  
105 leaves of dark- and light-adapted *A. thaliana* plants.

106

## 107 **Materials and Methods**

### 108 ***Plant Material***

109 *A. thaliana* (Col-0) was grown for 6-8 weeks in soil in a 8h light ( $140 \mu\text{mol photons m}^{-2} \text{s}^{-1}$ ),  
110  $22^\circ\text{C}/16\text{h dark}$ ,  $18^\circ\text{C photoperiod}$ . Spinach was purchased at a local market.

111

### 112 ***Construction of GFP reporter plasmids for stable expression in Arabidopsis thaliana***

113 To express PTOX:GFP fusion in *A. thaliana* wild type, we PCR-amplified the entire sequence  
114 of *PTOX* using the primers *SalI-N-ter* (CTGGTCGACATGGCGGCGATTTCAGG) and *NcoI-*  
115 *C-ter* (TTCCCATGGAAGTTGTAATGGATTTCTTGAG) from an *A. thaliana* cDNA library.  
116 The PCR product was cloned into the pBluescript KS<sup>-</sup> vector (Stratagene). The *SalI-NcoI*  
117 fragment was inserted into the *SalI-NcoI* digested GFP reporter plasmid *Pro35S:sGFP(S65T)* to  
118 create the *Pro35S:PTOX-sGFP(S65T)* plasmid. From this construct, we extracted the entire

119 cassette Pro<sub>35S</sub>-PTOX-GFP-Nos Ter using *EcoRI* and a partial *HindIII* digestion. This fragment  
120 was purified and inserted into the *EcoRI-HindIII* digested pEL103 binary vector (kanamycin  
121 resistance to transform wild-type plants). Correct orientation and sequence of the inserted  
122 fragments were controlled. Plasmids used for *Agrobacterium tumefaciens* transformation were  
123 prepared using the “NucleoSpin Plasmid Kit” (Macherey-Nagel; Germany). The protein level  
124 of the GFP:PTOX protein was about three times higher compared to the intrinsic PTOX protein  
125 (Supplementary material Fig. S1).

126

### 127 ***Preparation of crude membrane extract and thylakoid membranes***

128 Crude extracts: Arabidopsis leaves were infiltrated with uncouplers by placing the petioles into  
129 water solutions containing nigericin (1  $\mu\text{M}$ ), valinomycin (1  $\mu\text{M}$ ) or just water (control) for 4 h  
130 under low light (8  $\mu\text{mol photons m}^{-2}\text{s}^{-1}$ ). The ethanol concentration was 0.01% in all solutions.  
131 Leaves were then exposed for 30 min to high light (500  $\mu\text{mol photons m}^{-2}\text{s}^{-1}$ ). After short  
132 homogenization (10 s) in buffer (0.33 M sorbitol, 60 mM KCl, 10 mM EDTA, 1 mM MgCl<sub>2</sub>,  
133 25 mM HEPES pH 7.6 and protease inhibitor cocktail (Sigma-Aldrich, St-Louis, Missouri,  
134 United States)) and filtration through 4 layers of mull, the filtrate was separated by  
135 centrifugation (5 min x 3000g at 4°C) in a supernatant and a membrane fraction. The pellet was  
136 resuspended in small amounts of buffer and the chlorophyll concentration determined. Proteins  
137 in the supernatant were precipitated with trichloroacetic acid (TCA). 25% TCA (v/v) was added  
138 to the supernatants, 10 min incubated on ice, centrifuged (15000g) and the pellet washed 3  
139 times with ice-cold acetone. Finally the pellet was dried and resuspended in 0.1 M TRIS pH  
140 8.0, 4% SDS before diluting it with sample buffer for SDS-PAGE.

141 Thylakoid membranes: Spinach leaves were homogenized in a blender for 10 s using a buffer  
142 containing 0.33 M sorbitol, 60 mM KCl, 10 mM EDTA, 1 mM MgCl<sub>2</sub>, 25 mM MES, pH 6.1.  
143 The slurry was filtered through 4 layers of cheesecloth, and the filtrate was centrifuged 3000 x  
144 g for 3 min at 4°C. The supernatant was discarded, and the pellet was resuspended in 0.33 M  
145 sorbitol, 60 mM KCl, 10 mM EDTA, 1 mM MgCl<sub>2</sub>, 25 mM HEPES, pH 6.7. The suspension  
146 was centrifuged 3000g for 3 min at 4°C. This step was repeated once with 20mM KH<sub>2</sub>PO<sub>4</sub>,  
147 5mM MgCl<sub>2</sub> as resuspending buffer. Finally, the pellet was resuspended in 0.3 M sucrose,  
148 20mM KH<sub>2</sub>PO<sub>4</sub>, pH 7.6. Before the measurements, thylakoid membranes were incubated for 20  
149 s in the same buffer containing various concentrations of MgCl<sub>2</sub> or KCl.

150

### 151 ***Expression and purification of MBP-PTOX***

152 PTOX from *Oryza sativa* fused with the maltose-binding protein (MBP-OsPTOX) was  
153 expressed and purified according to Yu et al. (2014). MBP protein was expressed and purified  
154 in the same way using the empty plasmid.

155

### 156 ***Liposome preparation***

157 The thylakoid lipids monogalactosyldiacylglycerol (MGDG), digalactosyldiacylglycerol  
158 (DGDG), sulfoquinovosyldiacylglycerol (SQDG), phosphatidylglycerol (PG) and  
159 phosphatidylcholine (PC), were purchased from Larodan Fine Chemicals (Malmö, Sweden)  
160 and dissolved in chloroform. Lipids were mixed in the following relative molar ratios: 41.2%  
161 MGDG, 26.7% DGDG, 15.6% SQDG, 11.5% PG, and 5% PC (Natali et al., 2016). 140 µl lipids  
162 were mixed with 5.84 ml of chloroform. 500 µl of the solution was pipetted into a glass vial  
163 and the chloroform was slowly removed under N<sub>2</sub> vapor in order to form a thin film of lipids  
164 on the inner wall of the vial. Lipids were rehydrated (using 500 µl buffer (50 mM TRIS-HCl  
165 pH 8.0, 2 mM KCl or 20 mM KCl; 50 mM MES pH 6.5, 2 mM KCl or 20 mM KCl) and  
166 vortexed (three times, each 5 min). Extrusion was performed 3 times through a 0.2 µm filter  
167 using the Extrusion was performed 3 times through a 0.2 µm nuclepore membranes (Whatman,  
168 GE Healthcare) using a homemade extrusion setup leading to liposomes of about 100 nm as  
169 measured by dynamic light scattering (Nano-S, Malvern, Sysmex, Norderstedt, Germany). 20  
170 µl MBP-OsPTOX (1 mg protein ml<sup>-1</sup>) was added to 200 µl liposomes, vortexed, deposited on  
171 a sucrose gradient (30%/15%) and centrifuged at 30 000g, 1h, 4°C. 200 µl were collected from  
172 the top of the gradient and used for further analyses.

173

### 174 **SDS-Page and Immunoblots**

175 PTOX and MBP binding to liposomes were resolved by SDS-PAGE (12%) and proteins were  
176 detected using Coomassie Brilliant Blue G250. Protein quantification was done using the  
177 Bradford reagent in case of chlorophyll free samples. Protein quantification in chlorophyll  
178 containing samples was done using Amidoblack.

179 Proteins were separated by SDS-PAGE (12% acrylamide) and immunoblotting using a  
180 nitrocellulose membrane. Labelling of the membranes with anti-PTOX antibody raised against  
181 the Arabidopsis protein (Josse et al., 2000) and anti-RuBisCo large subunit (RBCL) antibody  
182 Agrisera, Vännäs, Sweden) was carried out at room temperature in 50 mM Tris-HCl pH 7.6,  
183 150 mM NaCl, 0.1% Tween-20 and 5% non-fat milk powder. After washing, bound antibodies  
184 were revealed with a peroxidase-linked secondary anti-rabbit antibody (Agrisera, Vännäs,  
185 Sweden) and visualized by enhanced chemiluminescence.

186

### 187 **Chlorophyll fluorescence**

188 Room temperature chlorophyll fluorescence was measured using a pulse-amplitude modulation  
189 fluorometer (DUAL-PAM, Walz, Effeltrich, Germany). The intensity of the measuring light  
190 was sufficiently low so that no increase in the fluorescence ( $F_0$ ) was observed. Prior to the  
191 measurement, the samples, containing  $20 \mu\text{g chl ml}^{-1}$  and  $1.5 \mu\text{g ml}^{-1}$  MBP-OsPTOX were dark-  
192 adapted for 1 min. Fluorescence induction was measured using a multiple turnover flash  
193 (duration 300 ms).

194

### 195 **Confocal laser scanning microscopy**

196 4 weeks old *A. thaliana* plants expressing GFP-PTOX were used for confocal fluorescence  
197 microscopy. Plants were either incubated in red light ( $150 \mu\text{mol quanta m}^{-2}\text{s}^{-1}$ ) for 30 min or  
198 dark-adapted before mounting leaves for microscopy. In case of measurements using uncoupler,  
199 images of the non-treated leaves were first registered and then  $1 \mu\text{M}$  nigericin was soaked under  
200 the cover slip. Alternatively, the petioles were placed in a  $1 \mu\text{M}$  nigericin solution and nigericin  
201 was taken up by the transpiration flow during 2 h. 8-bit Images of biological samples and 100  
202 nm yellow-green and orange fluorescent beads (Fluospheres Carboxylate-modified  
203 microspheres, Thermofisher) were collected using a Leica 63x oil immersion objective (HCX  
204 Plan APO CS, NA 1.4, working distance 0.14 mm) with an inverted Leica laser-scanning  
205 confocal microscope TCS SP5 II (Leica Microsystems, Heidelberg, Germany) equipped with a  
206 GaAsP hybrid detection system at Nyquist sampling rate, with the detection pinhole aperture  
207 adjusted to 0.6 Airy units. Scanning was performed at 400 Hz. GFP and chlorophyll  
208 fluorescence was detected using laser lines 488 nm and 633 nm, respectively. Detections ranges  
209 were set for GFP (495 nm-560 nm) and chlorophyll (644 nm-718 nm). For excitation of GFP  
210 fluorescence laser power between 0.15 and 0.3 mW were chosen (Fig. 4, light: 0.15 mW; dark:  
211 0.28 mW; Fig. 5, H<sub>2</sub>O: 0.23 mW; H<sub>2</sub>O/Nig: 0.23 mW; Nig: 0.3 mW; Tables 2 and 3: 0.3 mW).  
212 For chlorophyll fluorescence laser power was adapted to signal strength (Fig. 4: 1.1 mW; Fig.  
213 5, H<sub>2</sub>O: 0.38 mW; H<sub>2</sub>O/Nig: 0.38 mW; Nig: 0.18 mW; Tables 2 and 3: 0.46 mW). For the  
214 detection systems the same gain was chosen for all images (16% for GaAsP hybrid detector and  
215 711 V for the photomultiplier tube. Imaging was performed in a temperature-controlled room  
216 at 21°C.

217 Deconvolution and image treatment: Confocal images of beads and biological data were  
218 deconvoluted with the Huygens 3.7 software (Scientific Volume Imaging, Hilversum,  
219 Netherlands) using a measured PSF using the Good's (GMLE) algorithm and a signal to noise



220 ratio of 15 as described in Lam et al. (2017). 3D reconstructions of deconvoluted datasets were  
221 carried out with ARIVIS VISION 4D-software.

## 222 **Results**

223 Previously we reported that PTOX was strongly attached to thylakoid membranes when  
224 Arabidopsis leaves had been exposed to high light intensity while it was only weakly attached  
225 in leaves incubated in the dark and we hypothesized that PTOX attachment to the membrane  
226 depends on the proton motive force (Feilke et al., 2016; Krieger-Liszkay and Feilke, 2016). To  
227 show whether the PTOX attachment in the light depends indeed on the proton motive force  
228 (pmf), we investigated the effect of uncouplers on the association of PTOX to the thylakoid  
229 membrane. We choose the uncouplers valinomycin and nigericin. Unlike valinomycin, a  
230 potassium-selective ionophore that dissipates  $\Delta\psi$ , nigericin abolishes both  $\Delta\text{pH}$  and  $\Delta\psi$   
231 (Nicholls and Ferguson, 2013). As shown in Fig. 1, less PTOX protein was found in the  
232 membrane fractions when leaves had been infiltrated with uncouplers prior to high light  
233 exposure. Consistently, more PTOX protein was found in the soluble protein fraction when the  
234 leaves had been treated with uncouplers. As loading control RuBisCo was used, that was present  
235 in small amounts in the membrane fraction and in large amounts in the fraction of the soluble  
236 proteins. No statistically significant difference was found between the two uncouplers used,  
237 nigericin and valinomycin. According to the results shown in Fig. 1, the pmf seems to be  
238 important for a strong attachment of PTOX to the thylakoid membrane.

239 To study in vitro the dependency of PTOX association to the thylakoid membrane on  
240 pH value and ion concentration, two approaches were employed using recombinant purified  
241 MBP-OsPTOX. In the first approach PTOX affinity to liposomes was investigated, while in the  
242 second approach thylakoid membranes were used instead of liposomes. In the first approach  
243 PTOX was added to liposomes prepared from a lipid mixture that mimics the lipid composition  
244 of the thylakoid membrane. Liposomes were rehydrated in buffers at pH 8.0 or pH 6.5 at two  
245 different potassium ion concentrations. pH 8.0 and pH 6.5 were chosen to simulate the pH  
246 values that face the thylakoid membrane in the light: slightly alkaline pH in the stroma and  
247 slightly acidic pH in the lumen. PTOX attachment to the liposomes was stronger at pH 8.0 than  
248 at pH 6.5 (Figure 2), indicating that the membrane association of PTOX is more favorable at  
249 slightly alkaline conditions. Furthermore, PTOX attachment at both pH values was stronger in  
250 the presence of 2 mM KCl than 20 mM KCl. One representative gel from four is shown in Fig.  
251 2. The recombinant PTOX protein used in the present study is a fusion protein between PTOX  
252 and the maltose-binding protein MBP. To exclude that the different binding properties of the  
253 recombinant protein to liposomes are due to MBP instead of PTOX properties, the same type  
254 of experiment was performed with MBP alone (SI Fig. 2). When one compares the protein  
255 amounts before and after the sucrose gradient in Fig. 2 and SI Fig. 2, MBP binding was much

256 lower than that of MBP-OsPTOX and did neither depend on the ion concentration nor on the  
257 pH-value. Therefore we conclude that it was indeed the binding of PTOX that was sensitive to  
258 both, the pH value and the ion concentration. Next, we investigated whether the lipid  
259 composition of the liposomes influenced the attachment of PTOX. When the charged lipids PG  
260 or SQDG were omitted from the liposomes, no difference in PTOX attachment was observed  
261 compared with the results obtained using liposomes prepared with the standard lipid  
262 composition (SI Fig. 3).

263 In the second approach MBP-OsPTOX was added to isolated thylakoid membranes.  
264 Binding was strongest in the presence of 1 mM MgCl<sub>2</sub> and decreased at higher MgCl<sub>2</sub>  
265 concentrations (Fig. 3). Fv/Fm values were similar at 1 mM and at 5 mM MgCl<sub>2</sub>, indicating  
266 that the same degree of stacking of the thylakoid membranes (Barber et al., 1980) was obtained  
267 with the two MgCl<sub>2</sub> concentrations (Table 1). When KCl was used instead of MgCl<sub>2</sub>, a weaker  
268 binding was observed at 20 mM KCl than at 2 mM KCl or in the absence of added KCl. Binding  
269 of MBP-OsPTOX to the thylakoid membrane without addition of salts may be either due to the  
270 ion concentration in the thylakoid membranes remaining from the preparation or to residual  
271 binding independent of the ionic strength of the medium. PTOX activity was monitored by  
272 chlorophyll fluorescence induction (SI Fig. 4). Addition of MBP-OsPTOX affected  
273 fluorescence induction at pH 8.0 but not at pH 6.5.

274 We used GFP-labelled AtPTOX expressed in *Arabidopsis thaliana* and confocal  
275 fluorescence microscopy to investigate changes in PTOX localization between light-adapted  
276 and dark-adapted chloroplasts. Expression of GFP-PTOX led to a faster quenching of variable  
277 chlorophyll fluorescence upon onset of actinic light but had little effect on photochemical  
278 quenching and non-photochemical quenching when measured on non-stressed plants taken  
279 from the growth cabinet (SI Fig. 5). Localization of the GFP fluorescence changed in the  
280 chloroplasts when chloroplasts from high light-treated and dark-adapted plants were compared  
281 as shown in Fig. 4 for chloroplasts of guard cells. In light-adapted plants GFP fluorescence was  
282 homogenously distributed over the whole chloroplasts while in dark-adapted plants GFP  
283 fluorescence was visible as characteristic spots restricted to small areas at the outer edges of the  
284 chloroplasts. Infiltrating leaves of high light exposed plants with nigericin led also to a more  
285 spotted distribution of the GFP fluorescence than observed in the absence of the uncoupler as  
286 shown in Fig. 5. In chloroplasts of wild-type plants no green autofluorescence spots were seen  
287 using the same setting of the microscope (SI Fig. 6). The analysis of more than hundred  
288 chloroplasts shows a large increase in chloroplasts with spots of GFP fluorescence in the  
289 presence of nigericin compared to a more homogenous distribution in the absence of the

290 uncoupler (Table 2). Next we analyzed the size of the GFP fluorescence spots (Table 3). The  
291 majority of the volume of the spots was smaller than  $100 \mu\text{m}^3$ , however, also much larger spots  
292 were found. Spot size distribution is heterogeneous with average volume ranges from  
293  $0.034 \pm 0.008$  to  $0.687 \pm 0.159 \mu\text{m}^3$ .

294

295

## 296 **Discussion**

297

### 298 **Effect of pH and ionic strength on the attachment of PTOX to the membrane**

299 Using leaves, thylakoid membranes and liposomes, we demonstrated here that the association  
300 of PTOX to the membrane was affected by uncouplers (Fig. 1, 5), by pH and by ion  
301 concentration (Figs 2, 3). According to our hypothesis, association of PTOX with the membrane  
302 is required to allow the access to its lipophilic substrate plastoquinol. A temporary, reversible  
303 attachment to the membrane is known to regulate the activity of certain enzymes. A change in  
304 pH, inducing protonation/deprotonation and in parallel, a change in the protein charge, induces  
305 for example membrane binding of hisactophilin, a cytoskeletal linker protein in Dictyostelium  
306 (Scheel et al., 1989). Another example of an enzyme known to associate with the thylakoid  
307 membrane in a pH-dependent manner is the violaxanthin de-epoxidase (Hager and Holocher,  
308 1994; Hieber et al., 2002). The pH value of the stroma is known to increase upon illumination  
309 (Heldt et al., 1973), and the light-induced proton increase in the lumen is electrically  
310 counterbalanced by ion fluxes through  $\text{Cl}^-$  (Schönknecht et al., 1988) and  $\text{K}^+$ -channels (Tester  
311 and Blatt, 1989; Carraretto et al., 2013). We suppose that both, the pH value and the ion  
312 concentration, are crucial for the attachment of PTOX with the membrane since both uncouplers  
313 nigericin and valinomycin led to a dissociation of a fraction of PTOX from thylakoid  
314 membranes in infiltrated leaves (Fig 1). According to reconstitution experiments using  
315 liposomes or isolated thylakoid membranes and recombinant Os-PTOX fused with the maltose  
316 binding protein, a more alkaline pH and a KCl or  $\text{MgCl}_2$  concentration in the lower millimolar  
317 range favoured the attachment of PTOX to the membrane (Figs 2, 3). We propose that lowering  
318 the pH from 8.0 to 6.5 induces either a conformational change in the PTOX protein structure  
319 that leads to a dissociation of the protein from the membrane or leads to protonation of amino  
320 acid residues that provide positive charges that are crucial for the membrane association. Since  
321 PTOX attachment is stronger at pH 8.0 than at pH 6.5 we suppose that PTOX is active at the  
322 stroma facing side of the membrane.

323

324 PTOX like AOX, the alternative oxidase of the mitochondria, is composed of a four-  
325 helix bundle that harbors the chelating sites for the diiron center and of two additional  
326 amphipathic helices that dock to one of the leaflets of the membrane (Nawrocki et al., 2015).  
327 Compared to the sequence of PTOX2 from *Chlamydomonas reinhardtii* that was used for  
328 modelling the membrane interaction by Nawrocki and co-workers, the length of the  
329 amphipathic helices is shorter in PTOX from higher plants and more similar in length to AOX.  
330 For AOX from *Trypanosoma brucei* a crystal structure is available (Shiba et al., 2013). The  
331 interaction of the AOX dimer with the membrane was modelled and, according to this model,  
332 five arginine residues are distributed along a boundary between the hydrophobic and  
333 hydrophilic regions of the dimer surface and the membrane. Several arginine residues are  
334 present in the predicted membrane association domains of the PTOX and may be important for  
335 the membrane association of the protein. They may interact with the negatively charged  
336 phospholipid head groups of the membrane. The arginine residues should remain charged at  
337 both pH values used here. Therefore, it seems more likely that a conformational change of the  
338 protein is responsible for its dissociation from the membrane at pH 6.5 than a protonation of an  
339 amino acid that permits the anchoring of the protein with the membrane. Hydrophobic  
340 interactions may be also important for the interaction between the membrane and the PTOX.  
341 pH changes and changes in the ion concentration can affect this kind of interaction. A specific  
342 role of either SQDG or PQ on the PTOX interaction with the membrane can be excluded since  
343 omission of either of the charged lipids from the lipid mixture for liposome production did not  
344 affect PTOX affinity (Fig. SI 2).

345

#### 346 **Localization of PTOX in the chloroplast**

347 Confocal microscopy data suggest that there is a pool of soluble PTOX that accumulates in  
348 spots in the dark while in the light PTOX is more homogenously distributed in a kind of network  
349 among the thylakoid membranes. Further investigations are needed to understand the nature of  
350 the PTOX accumulation/dissociation. We propose a dynamic model of PTOX localization  
351 inside the chloroplast: If the proton gradient across the membrane reaches a certain threshold  
352 value, PTOX moves to the margin region or the grana stacks of the thylakoid membrane where  
353 it has access to its substrate and fulfills its function keeping the redox state of the PQ pool  
354 poised. Under conditions of a lower proton motive force it detaches from the membrane or  
355 localizes in parts of the membrane system where it is inactive in respect to photosynthetic  
356 electron transport. In the light, an increase in pH and in ion concentration in the stroma may  
357 dissolve PTOX spots and facilitate the binding of PTOX to the membrane. In addition to soluble

358 PTOX, PTOX seems to be located in its resting state in high concentrations at the stroma  
359 lamellae or in specific membrane domains seen as spots by confocal microscopy. The  
360 diffraction-limited resolution of confocal microscopy does not allow to distinguish between  
361 spots in the stroma and spots that are formed at a specific membrane domain. Stepien and  
362 Johnson (2018) showed that PTOX overexpressed in *Eutrema salsugineum* moved from the  
363 stroma lamellae to the grana stacks upon exposure to salt stress. Such a movement is consistent  
364 with our model, however, accumulation of PTOX in high concentrations at the stroma lamellae  
365 are required to explain the spot formation. In contrast to Stepien and Johnson (2018) who  
366 proposed that PTOX translocates in an unknown way from the stroma-facing side to the luminal  
367 side of the membrane and that it is active in the thylakoid lumen, our data suggest that PTOX  
368 is active at the stromal side of the membrane at slightly alkaline pH values.

369 The different distribution of PTOX within the chloroplast may be caused by both,  
370 differences in the ratio between membrane-bound PTOX and soluble PTOX and by different  
371 oligomerization states of PTOX. PTOX may accumulate in high concentrations in its soluble  
372 form forming the spots and may dissociate into smaller units upon changes in pH and binding  
373 to the membrane. These spots may be part of a cellular structure that contains not only PTOX  
374 in high concentration but also other components and proteins. A large part of the spots falls into  
375 the size category of a known specific cellular structure, namely plastoglobuli. Plastoglobuli  
376 have a diameter of 45 to 60 nm (Austin II et al., 2006) in chloroplast of non-stressed plants.  
377 However, also smaller and larger PTOX spots were found in the chloroplasts analyzed here.  
378 Furthermore, the spot size does not increase upon light stress (SI Fig. 7). This finding does not  
379 correlate well with plastoglobuli. Most probably, the GFP spots represent accumulations of  
380 PTOX in a structure of variable size different to regular plastoglobuli.

381 The catalytically functional unit of PTOX consists most likely of a dimer as it is the case  
382 for AOX (Shiba et al., 2013). MBP-OsPTOX tends to form different oligomeric states  
383 depending on the used detergent. In the presence of n-octyl  $\beta$ -D-glucopyranoside MBP-PTOX  
384 was found mainly as a tetramer (Yu et al., 2014) while it was mainly in a dimeric form in the  
385 presence of  $\beta$ -dodecyl-maltoside (SI Fig. 8). The native protein and the GFP-fusion protein may  
386 form larger oligomers than MBP-PTOX, since fusion with MBP increases the solubility of the  
387 protein. Different oligomerization states of phytoene desaturase, an enzyme of the carotenoid  
388 biosynthesis pathway, have been reported previously. This enzyme does exist in a soluble form  
389 and in a membrane-associated form where it has access to its lipophilic substrate. Phytoene  
390 desaturase forms higher order oligomeric species with two distinguishable structures consisting  
391 either of rings or stacks (Gemmecker et al., 2015). Rings were ascribed to a tetramer which

392 assembled into stacked tubular structures of a length between 15–30 nm. The stacks represented  
393 the soluble form while the active form attached to liposomes was a single tetrameric ring.

394 Knowledge about the geometry of the membrane system is required to understand  
395 relocalization of a protein like PTOX. Higher plant thylakoid membranes are organized in grana  
396 stacks, composed of cylindrical stacked membranes of 350-600 nm in diameter, interconnected  
397 by unstacked stroma lamellae, and forming a continuous complex structured membrane  
398 network that separates the thylakoid lumen from the stroma. It has been observed that the  
399 overall thylakoid architecture is highly dynamic (Kirchhoff, 2019; Pribil et al., 2014). It is likely  
400 that changes in the size of the lumen or a partial destacking of grana control transport processes  
401 within the thylakoid membrane system and may control also the localization of proteins in the  
402 stroma which is densely packed with proteins. In the light, the building up of the proton motive  
403 force may cause swelling of the lumen induced by influx of protons into the lumen (Kirchhoff  
404 et al., 2011; Ruban and Johnson, 2015) and may affect thereby protein localization in the  
405 stroma. The ion concentration in the stroma increases when the proton motive force is high. A  
406 change of the ion concentration in the stroma may affect the solubility of proteins, the stability  
407 of larger protein complexes and may allow the accumulation of PTOX in spots.

408 Further studies are required to get insights into the arrangement of PTOX at the  
409 membrane, to understand the mechanism behind PTOX accumulation into spots, to investigate  
410 whether other proteins or lipids than PTOX are present in the spots and to study whether PTOX  
411 activity correlates with its distribution (network-like structure versus spots) within the  
412 chloroplast.

413

414

#### 415 **Acknowledgements**

416 A.K.L., E. M., M. J. and M.P. benefit from the support of the LabEx Saclay Plant Sciences-SPS  
417 (ANR-10-LABX-0040-SPS) and the French Infrastructure for Integrated Structural Biology  
418 (FRISBI) ANR-10-INSB-05.

419 **References**

- 420
- 421 **Austin II JR, Frost E, Vidi PA, Kessler F Staehelin LA.** 2006. Plastoglobules are lipoprotein  
 422 subcompartments of the chloroplast that are permanently coupled to thylakoid membranes  
 423 and contain biosynthetic enzymes. *Plant Cell* **18**, 1693-1703.  
 424 <https://doi.org/10.1105/tpc.105.039859>
- 425 **Barber J., Chow W.S., Scoufflaire C., Lannoye R.** 1980. The relationship between thylakoid  
 426 stacking and salt induced chlorophyll fluorescence changes. *Biochimica et Biophysica Acta*  
 427 **591**, 92-103. [https://doi.org/10.1016/0005-2728\(80\)90223-6](https://doi.org/10.1016/0005-2728(80)90223-6)
- 428 **Carol P, Stevenson D, Bisanz C, Breitenbach J, Sandmann G, Mache R, Coupland G,**  
 429 **Kuntz M.** 1999. Mutations in the Arabidopsis gene IMMUTANS cause a variegated  
 430 phenotype by inactivating a chloroplast terminal oxidase associated with phytoene  
 431 desaturation. *Plant Cell* **11**, 57–68. <https://doi.org/10.1105/tpc.11.1.57>
- 432 **Carraretto L, Formentin E, Teardo E, Checchetto V, Tomizioli M, Morosinotto T,**  
 433 **Giacometti, GM, Finazzi G, Szabó I.** 2013. A thylakoid-located two-pore K<sup>+</sup> channel  
 434 controls photosynthetic light utilization in plants. *Science* **342**, 114–118.  
 435 <https://doi.org/10.1126/science.1242113>
- 436 **Feilke K, Streb P, Cornic G, Perreau F, Kruk J, Krieger-Liszkay A.** 2016. Effect of  
 437 *Chlamydomonas* plastid terminal oxidase 1 expressed in tobacco on photosynthetic electron  
 438 transfer. *Plant Journal* **85**, 219-228. <https://doi.org/10.1111/tpj.13101>
- 439 **Gemmecker S, Schaub P, Koschmieder J, Brausemann A, Drepper F, Rodriguez-Franco**  
 440 **M, Ghisla S, Warscheid B, Einsle O, Beyer P.** 2015. Phytoene Desaturase from *Oryza*  
 441 *sativa*: Oligomeric Assembly, Membrane Association and Preliminary 3D-Analysis. *PLoS*  
 442 *One*. **10**:e0131717. <https://doi.org/10.1371/journal.pone.0131717>
- 443 **Hager A, Holocher K.** 1994. Localization of the xanthophyll-cycle enzyme violaxanthin de-  
 444 epoxidase within the thylakoid lumen and abolition of its mobility by a (light-dependent) pH  
 445 decrease. *Planta* **192**, 581–589. <https://doi.org/10.1007/BF00203597>
- 446 **Heldt HW, Werdan K, Milovancev M, Geller G.** 1973. Alkalization of the chloroplast stroma  
 447 caused by light-dependent proton flux into the thylakoid space. *Biochimica Biophysica Acta*  
 448 **314**, 224–241. [https://doi.org/10.1016/0005-2728\(73\)90137-0](https://doi.org/10.1016/0005-2728(73)90137-0)
- 449 **Hieber AD, Bugos RC, Verhoeven AS, Yamamoto HY.** 2002. Overexpression of  
 450 violaxanthin de-epoxidase: properties of C-terminal deletions on activity and pH-dependent  
 451 lipid binding. *Planta* **214**, 476–483. <https://doi.org/10.1007/s00425-001-0704-2>
- 452 **Ivanov, AG, Rosso D, Savitch LV, Stachula P, Rosembert M, Oquist G, Hurry V, Hüner**  
 453 **NPA.** 2012. Implications of alternative electron sinks in increased resistance of PSII and PSI  
 454 photochemistry to high light stress in cold-acclimated *Arabidopsis thaliana*. *Photosynthesis*  
 455 *Research* **113**, 191–206. <https://doi.org/10.1007/s11120-012-9769-y>
- 456 **Josse EM, Simkin AJ, Gaffé J, Labouré AM, Kuntz M, Carol P.** 2000. A plastid terminal  
 457 oxidase associated with carotenoid desaturation during chromoplast differentiation. *Plant*  
 458 *Physiol* **123**, 1427-1436. <https://doi.org/10.1104/pp.123.4.1427>
- 459 **Ruban AV, Johnson MP.** 2015. Visualizing the dynamic structure of the plant  
 460 photosynthetic membrane. *Nature plants* **1**,15161. <https://doi.org/10.1038/nplants.2015.161>
- 461 **Kirchhoff H, Hall C, Wood M, Herbstová M, Tsabari O, Nevo R, Charuvi D, Shimoni E,**  
 462 **Reich Z.** 2011. Dynamic control of protein diffusion within the granal thylakoid lumen.  
 463 *Proceedings of the National Academy of Sciences U S A* **108**, 20248-20253.  
 464 <https://doi.org/10.1073/pnas.1104141109>
- 465 **Kirchhoff H.** 2019. Chloroplast ultrastructure in plants. *New Phytologist* **223**, 565-574.  
 466 <https://doi.org/10.1111/nph.15730>



467 **Krieger-Liszkay A, Feilke K.** 2016. The dual role of the Plastid Terminal Oxidase PTOX:  
468 Between a protective and a pro-oxidant function. *Frontiers in Plant Science* **6**,1147.  
469 <https://doi.org/10.3389/fpls.2015.01147>

470 **Lam F, Cladière D, Guillaume C, Wassmann K, Bolte S.** 2017. Super-resolution for  
471 everybody: An image processing workflow to obtain high-resolution images with a standard  
472 confocal microscope. *Methods* **115**, 17-2. <https://doi.org/10.1016/j.ymeth.2016.11.003>

473 **Laureau C, De Paepe R, Latouche G., Moreno-Chacón M, Finazzi G, Kuntz M, Cornic  
474 G, Streb P.** 2013. Plastid terminal oxidase (PTOX) has the potential to act as a safety valve  
475 for excess excitation energy in the alpine plant species *Ranunculus glacialis* L. *Plant Cell &  
476 Environment* **36**, 1296–1310. <https://doi.org/10.1111/pce.12059>

477 **Lennon AM, Prommeenate P, Nixon PJ.** 2003. Location, expression and orientation of the  
478 putative chlororespiratory enzymes, ndh and immutans, in higher-plant plastids. *Planta* **218**,  
479 254–260. <https://doi.org/10.1007/s00425-003-1111-7>

480 **Natali A, Gruber JM, Dietzel L, Stuart MCA, van Grondelle R, Croce R.** 2016. Light-  
481 harvesting complexes (LHC) cluster spontaneously in membrane environment leading to  
482 shortening of their excited state lifetimes. *Journal of Biological Chemistry* **291**, 16730-  
483 16739. <https://doi.org/10.1074/jbc.M116.730101>

484 **Nawrocki WJ, Tourasse NJ, Taly A, Rappaport F, Wollman FA.** 2015. The plastid terminal  
485 oxidase: its elusive function points to multiple contributions to plastid physiology. *Annual  
486 Reviews of Plant Biology* **66**, 49–74. <https://doi.org/10.1146/annurev-arplant-043014-114744>

488 **Nicholls DG, Ferguson SJ.** 2013. *Bioenergetics*. 4<sup>th</sup> edition. London: Academic Press, London  
489 UK, p. 19

490 **Ollion J, Cochennec J, Loll F, Escudé C, Boudier T.** 2013. TANGO: A Generic Tool for  
491 High-throughput 3D Image Analysis for Studying Nuclear Organization. *Bioinformatics* **29**,  
492 1840-1841. <https://doi.org/10.1093/bioinformatics/btt276>

493 **Pribil M, Labs M, Leister D.** 2014. Structure and dynamics of thylakoids in land plants.  
494 *Journal of Experimental Botany* **65**, 1955-1972. <https://doi.org/10.1093/jxb/eru090>

495 **Quiles MJ.** 2006. Stimulation of chlororespiration by heat and high light intensity in oat plants.  
496 *Plant Cell & Environment* **29**, 1463–1470. <https://doi.org/10.1111/j.1365-3040.2006.01510.x>

498 **Schönknecht G, Hedrich R, Junge W, Raschke K.** 1988. A voltage-dependent chloride  
499 channel in the photosynthetic membrane of a higher plant. *Nature* **336**, 589–592.  
500 <https://doi.org/10.1038/336589a0>

501 **Shiba T, Kido Y, Sakamoto K, Inaoka DK, Tsuge C, Tatsumi R, Takahashi G, Balogun  
502 EO, Nara T, Aoki T, Honma T, Tanaka A, Inoue M, Matsuoka S, Saimoto H, Moore  
503 AL, Harada S, Kita K.** 2013. Structure of the trypanosome cyanide-insensitive alternative  
504 oxidase. *Proceedings of the National Academy of Sciences U S A* **110**, 4580-4585.  
505 <https://doi.org/10.1073/pnas.1218386110>

506 **Stepien P, Johnson GN.** 2009. Contrasting responses of photosynthesis to salt stress in the  
507 glycophyte *Arabidopsis* and the halophyte *Thellungiella*: role of the plastid terminal oxidase  
508 as an alternative electron sink. *Plant Physiology* **149**, 1154–1165.  
509 <https://doi.org/10.1104/pp.108.132407>

510 **Tester M, Blatt MR.** 1989. Direct measurement of K channels in thylakoid membranes by  
511 incorporation of vesicles into planar lipid bilayers. *Plant Physiology* **91**, 249-252.

512 **Trouillard M, Shahbazi M, Moyet L, Rappaport F, Joliot P.A., Kuntz M., Finazzi G.** 2012.  
513 Kinetic properties and physiological role of the plastoquinone terminal oxidase (PTOX) in  
514 a vascular plant. *Biochimica et Biophysica Acta* **1817**, 2140–2148.  
515 <https://doi.org/10.1104/pp.91.1.249>

516 **Scheel J, Ziegelbauer K, Kupke T, Humbel BM, Noegel AA, Gerisch G, Schleicher M.**  
517 1989. Hisactophilin, a histidine-rich actin-binding protein from Dictyostelium discoideum.  
518 Journal of Biological Chemistry **264**, 2832–2839.

519 **Wetzel CM, Jiang CZ, Meehan LJ, Voytas DF, Rodermel SR.** 1994. Nuclear-organelle  
520 interactions: the immutans variegation mutant of Arabidopsis is plastid autonomous and  
521 impaired in carotenoid biosynthesis. Plant Journal **6**, 161–175.  
522 <https://doi.org/10.1046/j.1365-313X.1994.6020161.x>

523 **Yu Q, Feilke K, Krieger-Liszkay A, Beyer P.** 2014. Functional and molecular  
524 characterization of plastid terminal oxidase from rice (*Oryza sativa*). Biochimica et  
525 Biophysica Acta **1837**, 1284–1292. <https://doi.org/10.1016/j.bbabi.2014.04.007>

526  
527  
528  
529

530 **Table 1: PSII efficiency (Fv/Fm) at different ion concentrations**

531

532

salt concentration	Fv/Fm
no salt added	0.79±0.15
1 mM MgCl <sub>2</sub>	0.86±0.05
5 mM MgCl <sub>2</sub>	0.86±0.07
2 mM KCl	0.82±0.10
20 mM Kcl	0.82±0.10

533

534

535

536

537 Isolated thylakoid membranes were diluted to 20 µg chl ml<sup>-1</sup> in 0.3 sorbitol, 25 mM HEPES  
538 pH 7.6 containing the indicated concentration of MgCl<sub>2</sub> or KCl and chlorophyll fluorescence  
539 induction curves were measured using a saturating light pulse after 5 min dark adaptation.

540

541

542

543

544 **Table 2: Distribution of GFP-PTOX in leaves in water and in nigericin**

	water	nigericin
Number chloroplasts with spots	12	93
Number of chloroplasts counted	145	120
Images analyzed	14	13

545

546 Leaves were illuminated for 15 min on the microscope stage using the continuous light source  
547 of the microscope and additionally an LED lamp emitting at 650 nm ( $160 \mu\text{mol quanta m}^{-2}\text{s}^{-1}$ )  
548 before taking images. Nigericin was added by placing a drop in close proximity to the cover  
549 slip and letting it enter into the leaf by diffusion.

550

551 **Table 3 : Size-distribution of the GFP-PTOX spots in dark-adapted leaves**

552

Spot groups	volume ( $\mu\text{m}^3$ ) of spot groups	Average volume ( $\mu\text{m}^3$ ) per group	number of spots
1	0.023-0.049	0.034 $\pm$ 0.008	56
2	0.050-0.099	0.068 $\pm$ 0.012	62
3	0.100-0.149	0.124 $\pm$ 0.014	25
4	0.149-0.290	0.203 $\pm$ 0.042	28
5	0.300-0.490	0.357 $\pm$ 0.038	18
6	0.500-1.000	0.687 $\pm$ 0.159	7

553

554 Confocal image stacks of dark-adapted leaves were processed with ImageJ (3D-iterative  
555 thresholding plugin (Ollion et al., 2013) to calculate spot volumes of PTOX-GFP labeled  
556 structures.

557

558

559

560

561 Figure legends

562 **Figure 1. PTOX attachment depends on the proton motive force.**

563 Arabidopsis leaves were exposed for 30 min to high light ( $500 \mu\text{mol photons m}^{-2}\text{s}^{-1}$ ) in the  
564 absence or presence of  $1 \mu\text{M}$  uncouplers. Leaf extracts were separated by centrifugation into a  
565 membrane fraction and a fraction containing soluble proteins. PTOX content of the membrane  
566 fraction was analyzed by SDS-PAGE and immunoblotting. Gels were loaded based on  
567 chlorophyll content ( $10 \mu\text{g Chl}$  per lane). Upper panels: Representative blots; C: no addition;  
568 N: Nigericin; V: Valinomycin. Two different exposure times were used for the blot showing  
569 the supernatants to allow discrimination between the two bands. Lower panels densities of  
570 the PTOX band in the membrane fractions (left) and the soluble protein fraction (right) from  
571 uncoupler-treated leaves were normalized to the density of the band of control (mean  $\pm$  SE, 3  
572 blots, each with proteins from different preparations, were used for the statistical analysis.  
573 The significance level obtained by Student's t-test ( $P < 0.05$ ) is indicated by letters.

574

575 **Figure 2. PTOX attachment to liposomes as a function of pH and salt concentration.**

576 Purified recombinant MBP-OsPTOX protein ( $1 \mu\text{g protein}$ ) was adsorbed to liposomes. Not  
577 absorbed PTOX was removed by centrifugation using sucrose gradients and the PTOX  
578 content of the recovered liposomes was analyzed by SDS-Page and CBB staining. PTOX  
579 attachment is shown at pH 6.5 and pH 8.0 in the presence of 2 and 20 mM KCl, respectively.

580

581 **Figure 3. PTOX attachment to thylakoid membranes as a function of the  $\text{MgCl}_2$  or KCl**  
582 **concentration.**

583 Purified recombinant MBP-OsPTOX protein ( $1.5 \mu\text{g ml}^{-1}$ ) was adsorbed to spinach thylakoid  
584 membranes ( $10 \mu\text{g Chl ml}^{-1}$ ) at pH 7.6 at the indicated ion concentrations. The membranes  
585 were pelleted before deposition of the samples on the gel (SDS-PAGE). PTOX amounts were  
586 revealed by immunoblotting.

587

588 **Figure 4**

589 Confocal fluorescence microscopy of guard cells of *A. thaliana* expressing GFP-PTOX  
590 Confocal images of chloroplasts expressing GFP of plants exposed to light (light, upper panels)  
591 throughout the experiment and plants kept in the dark before imaging (dark, lower panels).  
592 Upper panels represent single fluorescence images (A) and 3-dimensional views of image  
593 stacks of control plants (A', A''). Lower panels represent single fluorescence images (B) and  
594 3-dimensional views of image stacks of plants kept in the dark (B', B'').

595 Fluorescent images (A, B) represent chlorophyll fluorescence (red) and GFP fluorescence  
596 (green) of stomata, with arrowheads marking the position of two chloroplasts shown in higher  
597 magnification below (a, a', b and b') and on the respective 3D-images. Scale bars are 5  $\mu\text{m}$ .  
598 Note the distribution of GFP in control plants (network) and dark treated plants (spots). Young  
599 leaves (3 week old plants) were chosen for the images.

600

### 601 **Figure 5**

602 Effect of the uncoupler nigericin on GFP-PTOX localisation in guard cells.

603 Leaves were exposed to red light ( $150 \mu\text{mol quanta m}^{-2}\text{s}^{-1}$ ) for 30 min.  $1 \mu\text{M}$  nigericin was  
604 soaked under the cover slip for the infiltrated leaves. Alternatively, the petioles were placed in  
605 a  $1 \mu\text{M}$  nigericin solution and nigericin was taken up by the transpiration flow during 2 h  
606 (incubated leaves). Scale bars are 5  $\mu\text{m}$ .

607

608

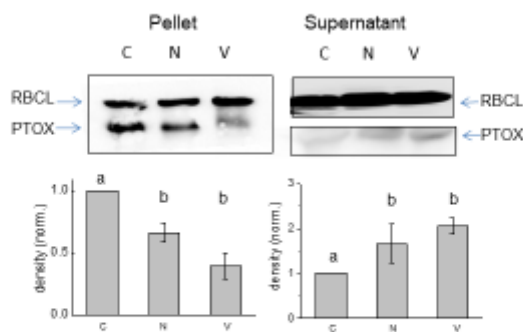


Figure 1. PTOX attachment depends on the proton motive force.

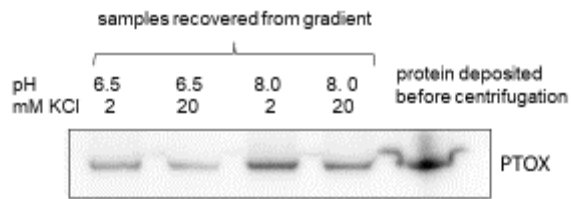


Figure 2. PTOX attachment to liposomes as a function of pH and ionic strength.

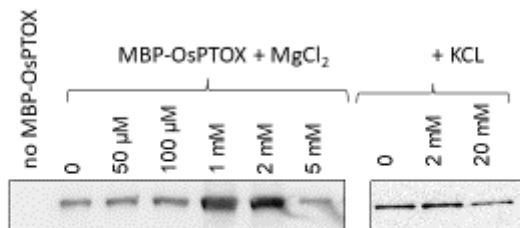


Figure 3. PTOX attachment to thylakoid membranes as a function of the MgCl<sub>2</sub> or KCl concentration.

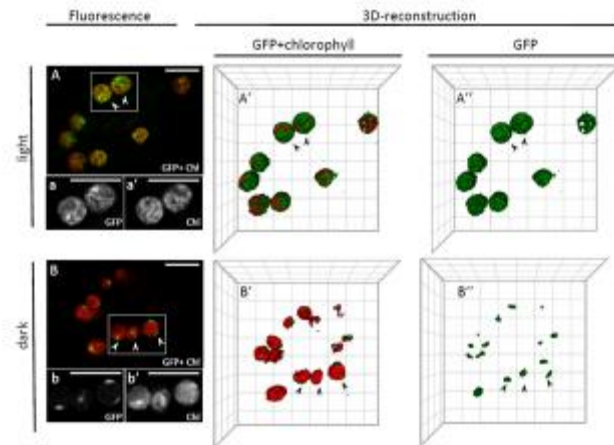


Figure 4. Confocal fluorescence microscopy of guard cells of *A. thaliana* expressing GFP-PTOX



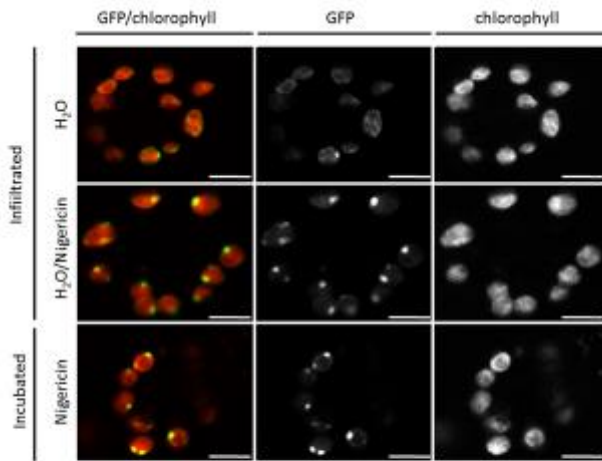


Figure 5. Effect of the uncoupler nigericin on GFP-PYOX localisation in guard cells.